Supporting information for "Nanoparticles dispersed in nematic liquid crystals: Impact on conductivtiy, low-frequency relaxation and electro-optical performance"

Martin Urbanski and Jan P. F. Lagerwall
Contact: Martin.Urbanski@lc-science.info

March 27, 2016

1   Alignment in LC test cells

Nematic liquid crystals are anisotropic materials in which many physical properties (e.g. permittivity ϵ, conductivity σ or refractive index n) differ for directions parallel or perpendicular to the uniaxial orientational order depicted by the director $\mathbf{n}$. The nematic host 4-cyano-4'-n-pentylbiphenyl (5CB) used in this study features a positive dielectric anisotropy $\left(\Delta\epsilon = \epsilon_\parallel - \epsilon_\perp > 0\right)$ and positive anisotropy of conductivity $\left(\Delta\sigma = \sigma_\parallel - \sigma_\perp > 0\right)$. The experimental results shown in this article depict $\epsilon_\perp$ and $\sigma_\perp$, as all measurments were performed perpendicular to the director. The LC alignment was achieved by using electro-optic LC test cells coated with polyimide alignment layers for planar alignment (KSRP-50/A111P1NSS by E.H.C. Co. Ltd, Japan). To ensure that the observed NP-induced increase of conductivity is not caused by nanoparticle-induced alignment changes[1], we tested the alignment of all samples by polarizing optical microscopy (cf. Figure 1).

The pristine host and dispersions of **NP1** show defect-free homogeneous planar alignment parallel to the rubbing direction of the polyimide alignment layers as indicated by the red bars. Only the test cell containing 0.05 % (w/w) **NP1** shows low residual birefringence between crossed polarizers for a sample orientation parallel to the polarizer. As areas showing homeotropic alignment would appear dark between crossed polarizers for any azimuthal orientation, we deduce that these domains show in-plane deviations from the rubbing direction, which should not affect the measurement of $\epsilon_\perp$ or $\sigma_\perp$.

Test cells filled with **NP2**-dispersions show numerous defects and inhomogeneties of alignment in an homogeneous planar environment. We therefore conclude that the experimental results for the conductivtiy of these samples might be affected by regions featuring the higher conductivtiy $\sigma_\parallel$, leading to a seemingly increased conductivity compared to the pristine host. However, such alignment effect would be orders of magnitude too small to explain the observed strong increase in conductivtiy for **NP2**-dispersions, so we are convinced that the dominating effect remains an increased number of mobile charge carriers.
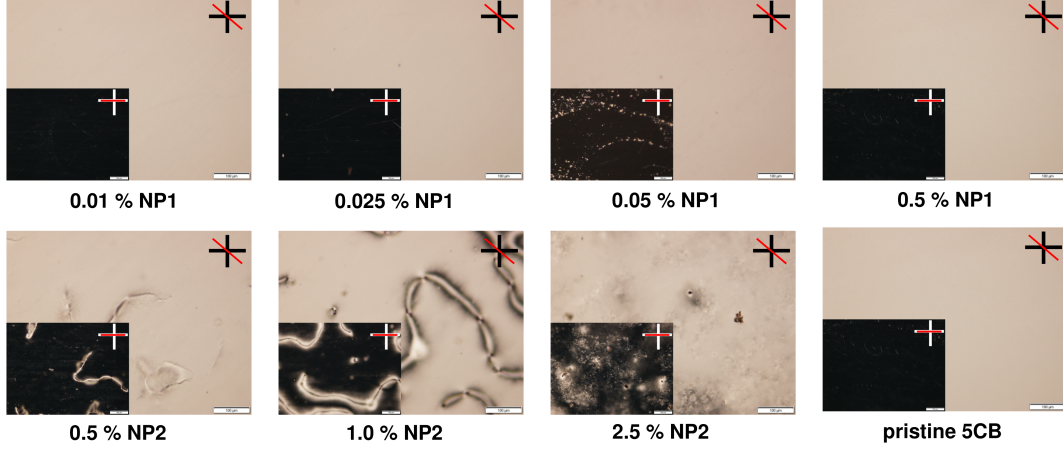
Figure 1: Polarizing optical microscopy images of pristine host, **NP1** and **NP2**-dispersions filled in 50 μm LC test cells with polyimide alignment layers for homogeneous planar alignment. The red bar represents the orientation of the PI rubbing direction with respect to the crossed polarizers, which are represented by the crossed back or white barsl, respectively.

2 Equivalent electrical circuit (EEC) model

The EEC model as shown in Fig. 2 in the main article was developed to be as simple as possible. The individual development steps for the final circuit are represented in Figure 2 and Figure 3 and underline that all components are inevitable to reproduce the experimental data with high accuracy. The simplest EEC used for modeling the impedance response of
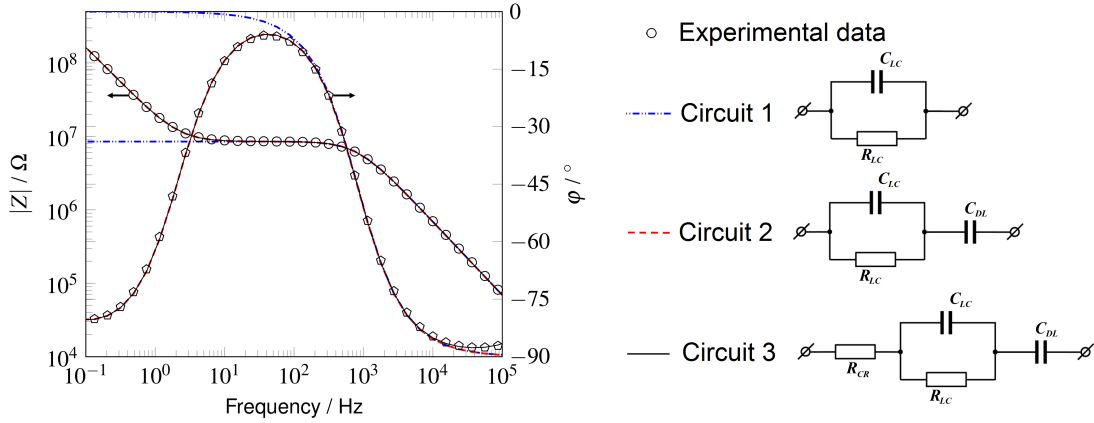

Figure 2: Summary of the development steps for a suitable equivalent electrical circuit (EEC) for test cells filled with NP-LC dispersions. Left: Experimental (open circles) and simulated (lines) impedance and phase angle response. Right: Schematic drawings of the respective EECs.

nematic LCs comprises a capacitor and a parallel-connected resistor (Circuit 1). Despite its simplicity, this circuit already reproduces the impedance response with high accuracy for frequencies from 10 Hz - 100 kHz and the phase angle for frequencies from 100 Hz - 30 kHz, covering all commonly used driving frequencies for LC devices. It fails, however, to model

the low frequency reactive behaviour with an increasing impedance and phase angles close to 0°. The model is therefore extended by a capacitor in series to the simple model circuit (Circuit 2), which is already sufficient to resolve the deviation in the low frequency regime and allows a accurate reproduction of experimental data. A further extension is required to also match the experimental phase angle response in the high frequency regime, in which the phase angle slightly increases towards an active resistance. This behaviour is caused by the finite resistance of connectors and electrodes and can be modeled by a resistor in series to circuit 2, resulting in circuit 3.

Although circuit 3 reproduced the experimental data shown in Figure 2 with high accuracy, a further extension is required due to diffusion occuring at low driving frequencies < 1 Hz. This can be seen in the Nyquist-representation of complex impedance shown in Figure 3: The relaxation mode of electrode polarization occurs at high frequencies, as depicted by the characteristic semi-circle in the inlet of Figure 3, while the low frequency response is given by a strong increase of the imaginary part $-Z''$ typical for diffusion processes. The EEC model 3 fails to reproduce this behavior (see dotted red line in Fig. 3), as it lacks a suitable component for modelling diffusion. A standard Warburg element for describing diffusion through the sample is found to be not suitable to reproduce the experimental data, as it yields a linear increase with a slope of +45° at low frequencies < 0.1 Hz (cf. dashed blue line in 3). We therefore extended the model by a generalized finite length Warburg element[2,3] as described in the main article, which considers the finite thickness of the LC test cell as a limiting factor for diffusion. This extended model as shown in Figure 2 in the main article is capable of reproducing the experimental data with reasonable accuracy (cf. black dashed line in Figure 3).
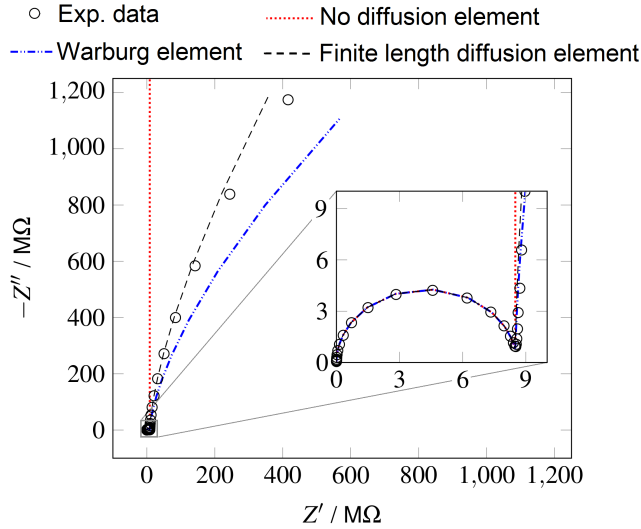

Figure 3: Nyquist representation of the complex impedance of pristine 5CB. The characteristic semi-circle in the inlet depicts electrode polarization, while the strong increase of the imaginary part $-Z''$ at low frequencies is caused by diffusion through the confined space in the liquid crystal test cell.

3 Effective Medium Approach for NP-LC Dispersions

Dispersions of metal nanoparticles in nematic liquid crystals can be considered as randomly structured media, in which the metal particles are arranged in a disordered fashion within the dielectric matrix . Despite permittivity inhomogeneities in the nm range, such composites represent homogeneous media on the macroscopic scale. Its effective permittivity can be obtained from the permittivities of its constituents and their respective volume fractions (Effective Medium Approach).

A suitable approach to describe the permittivity of NP-LC dispersions is given by the Maxwell-Garnett theory[4]: The nematic liquid crystal is considered as a dielectric host with the permittivity ϵ_{LC} and the nanoparticles are considered as inlcusion with a higher permittivity ϵ_{NP}. The overall volume filling factor ϕ of the conclusion is $\ll 1$ due to the limited dispersability of particles in the host material. An approximation for the effective permittivity is then given by equation 1:

$$\epsilon = \epsilon_{LC} + 3\phi_{NP}\epsilon_{LC}\frac{\epsilon_{NP} - \epsilon_{LC}}{\epsilon_{NP} + 2\epsilon_{LC}}. \tag{1}$$

A rough estimation of ϕ_{NP} for the nanoparticle dispersions investigated in this study is accessible by assuming the NPs to be perfectly dispersed and distribiuted within the LC host: For spherical gold particles with an average diameter of 4 nm, a core density of 19.32 g/cm^3 and a surface functionalization of 0.8 dodecanethiol molecules per surface atom[5,6], the average distance d between individual NPs and the overall metal volume filling factor ϕ can be estimated. The results are summarized in Figure 4 and clearly show that even for the highest doping concetrations used in this study, the volume filling factor $\phi_{NP} \approx 1 \cdot 10^{-3}$ is negligibly small. As seen from equation 1, it is therefore not expected that doping the host 5CB with up to 2.5 % (w/w) functionalized gold NPs will noticeably increase the effective permittivity of the dispersion compared to the prisitine host.
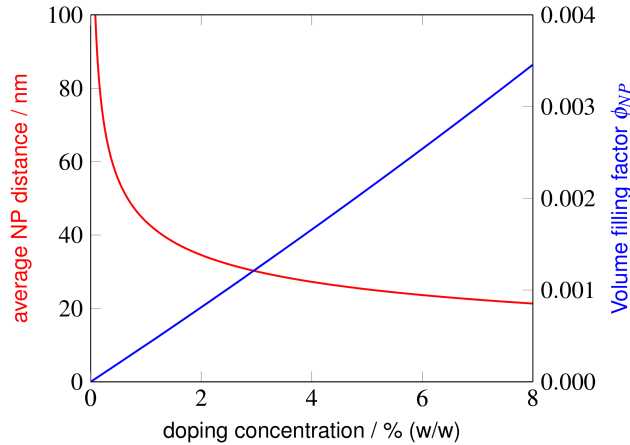

Figure 4: Plots of estimated average interparticle distance (red) and metal volume filling factor (blue) for ideally dispersed and distributed **NP1** in the nematic host 5CB.

4

4 Movie description "Visualization of Electrode Polarization in LC Test Cells"

The ion distribution (cf. screenshot in Figure 5, bottom) and E-field distribution (middle) within a dielectric slab under the influence of an external sinusoidal driving voltage of 25 mV (top) are shown for a driving frequency below the onset frequency of electrode polarization f_{EP} (left) and above this frequency (right). Calculations base on the approach by Coelho[7,8].
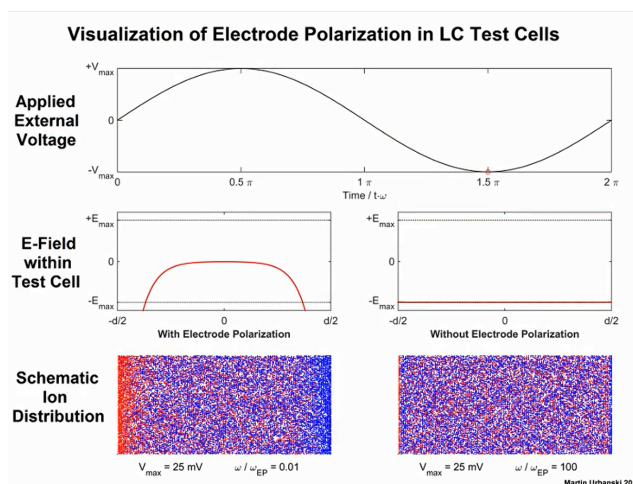

Figure 5: Example screenshot from the movie "Visualization of Electrode Polarization on LC Test Cells" in the ESI to this article.

The ion density is visualized by red and blue dots, representing anions and cations, respectively. At a low driving frequency ($\omega = 0.01\omega_{EP}$) ions noticeably accumulate in the vicinity of the electrodes, while no such observation can be made for a high driving frequency ($\omega = 0.01\omega_{EP}$). For the latter case the electric field within the testcell is constant through the cell gap, the field strength corresponds to $E = \frac{V}{d}$. The field distribution for the low driving frequency is dominated by a shielding of electric field by the accumulated space charge in the vicinity of the electrodes, so that the electric field in thie middle of the test cell almost vanishes completely. This shielding gives an explanation for the strong increase of threshold voltage, as demonstrated in Figure 5 in the main article.

References

[1] M. Urbanski, J. Mirzaei, T. Hegmann and H.-S. Kitzerow, *ChemPhysChem*, 2014, **15**, 1395–1404.

[2] J. Illig, *PhD thesis*, Karlsruher Institut für Technologie, 2014.

[3] B. A. Belyaev and N. A. Drokin, *Physics of the Solid State*, 2015, **57**, 181–187.

[4] *Optical Metamaterials*, ed. W. Cai and V. Shalaev, Springer, New York, 2010.

[5] J. Mirzaei, M. Urbanski, H.-S. Kitzerow and T. Hegmann, *ChemPhysChem*, 2014, **15**, 1381–1394.

[6] M. Draper, I. M. Saez, S. J. Cowling, P. Gai, B. Heinrich, B. Donnio, D. Guillon and J. W. Goodby, *Advanced Functional Materials*, 2011, **21**, 1260–1278.

[7] R. Coelho, *Revue Phys. Appl.*, 1983, **18**, 137–146.

[8] R. Coelho, *Journal of Non-Crystalline Solids*, 1991, **131-133**, 1136–1139.